Observed and projected declines in glacier albedo across the Third Pole in the 21st century

Ren, Shaoting; Jia, Li; Miles, Evan S.; Menenti, Massimo; Kneib, Marin; Shaw, Thomas E.; Buri, Pascal; McCarthy, Michael J.; Yang, Wei; Pellicciotti, Francesca

Important note
To cite this publication, please use the final published version (if applicable).
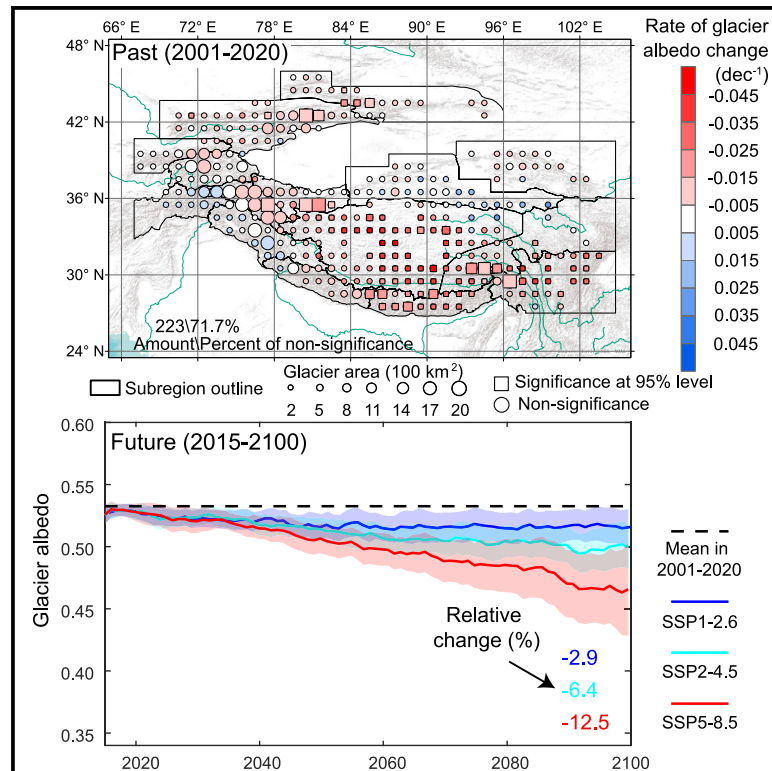Please check the document version above.

Observed and projected declines in glacier albedo across the Third Pole in the 21st century

Graphical abstract

Authors

Shaoting Ren, Li Jia, Evan S. Miles, ..., Wei Yang, Francesca Pellicciotti, Tandong Yao

Correspondence

jiali@aircas.ac.cn

In brief

Glacier albedo is a key control of glacier mass loss in the Third Pole, but its changes and potential drivers are still poorly quantified. Leveraging satellite-derived glacier albedo and newly developed albedo estimation models, this study reveals continuous glacier darkening in the 21st century and the associated mass loss. These findings highlight the key role of glacier albedo in enhancing future glacier ablation and the urgency of mitigating climate warming and atmospheric light-absorbing particles for the persistence of Asian glaciers.

Highlights

- Glacier albedo is highly variable across distinct subregions of the Third Pole

- Interannual variability belies long-term decreases in glacier albedo

- Air temperature and snow are primary drivers of changes in glacier albedo

- Third Pole glaciers will continue to darken during the 21st century

CellPress

Article

Observed and projected declines in glacier albedo across the Third Pole in the 21st century

Shaoting Ren,[1] Li Jia,[2,5,*] Evan S. Miles,[3] Massimo Menenti,[2,4] Marin Kneib,[3] Thomas E. Shaw,[3] Pascal Buri,[3] Michael J. McCarthy,[3] Wei Yang,[1] Francesca Pellicciotti,[3] and Tandong Yao[1]

[1]State Key Laboratory of Tibetan Plateau Earth System, Resources and Environment (TPESER), Institute of Tibetan Plateau Research, Chinese Academy of Sciences, Beijing, China
[2]Key Laboratory of Remote Sensing and Digital Earth, Aerospace Information Research Institute, Chinese Academy of Sciences, Beijing, China
[3]Swiss Federal Institute for Forest, Snow and Landscape Research WSL, Birmensdorf, Switzerland
[4]Faculty of Civil Engineering and Earth Sciences, Delft University of Technology, Delft, the Netherlands
[5]Lead contact
*Correspondence: jiali@aircas.ac.cn
https://doi.org/10.1016/j.oneear.2024.08.010

SCIENCE FOR SOCIETY Glaciers in the Third Pole (i.e., the Tibetan Plateau and its surroundings) supply more than a billion people with freshwater resources for societal, environmental, and economic needs, but they are shrinking. Glacier albedo, which measures how much solar radiation is reflected by a glacier, is a physical link between glacier changes and variations in climate and atmospheric particles. As glaciers darken, they absorb more energy, which has been identified as a key driver of glacier shrinkage in this region, possibly shaping future glacier trajectories. However, glacier albedo changes in the 21st century remain poorly understood. Using satellite observations, we find that glacier albedo has declined over 2001–2020 in most regions of the Third Pole, and the moderate and high warming scenarios imply strong further decreases by 2100, contributing to the continuing demise of Asian glaciers. These findings underline the importance of albedo in glacier projection and the urgency of mitigating climate warming.

SUMMARY

Glaciers are crucial water resources in the Third Pole (the Tibetan Plateau and its surroundings) and are shrinking in response to climate change. Glacier albedo is an expression of glacier interactions with climate and dust/black carbon, and albedo reduction enhances glacier mass loss, but its changes and potential drivers remain poorly quantified. We leverage satellite observations to explore the variability of glacier albedo and understand its sensitivity to potential drivers and its future evolution. We find that glacier albedo has declined during 2001–2020, but high interannual variability is also an important signal. These variations are highly sensitive to air temperature and snow conditions and to nearby dust/black carbon emission sources. Future changes to these drivers will lead to further decreases of 2.9%–12.5% in glacier albedo by 2100 under different warming scenarios. These findings highlight the importance of albedo in glacier future evolution and the urgency of action to mitigate climate warming.

INTRODUCTION

The Third Pole, including the Tibetan Plateau and surrounding Hindu Kush-Karakoram-Himalayan system, is home to approximately 100,000 km^2 of glaciers, the largest glacierized area outside of the north and south poles.[1,2] The runoff from these glaciers contributes to the water security of nearly one billion people and feeds major rivers and lakes in Asia[3,4]; hence, it is known as

the "water tower of Asia."[5] However, the Third Pole's glaciers have been shrinking in recent years,[6–9] with implications for terrestrial water cycle, ecosystem resilience, and food security.

Glacier albedo, the ratio of upward and downward shortwave radiation, is a physical link between climatic variability, glacier mass balance, and deposition of light-absorbing particles (primarily dust and black carbon).[10–17] Previous studies have shown that it changes spatially and temporally across the Third Pole,[1,5,9,18] and

the decline is known to be a key driver of glacier mass loss in this region.[15] Glacier albedo determines the net shortwave radiation that is absorbed by glacier surfaces throughout the region and,[19–22] therefore, is a key indicator of glacier persistence.[14,15,23,24] The glacier albedo feedback,[12] where decreases in albedo lead to glacier mass loss and further decreases in albedo, makes glaciers especially sensitive to climate change.

A number of compounding factors affect the glacier albedo in complex and nonlinear ways. Increasing temperature and precipitation changes from solid to liquid reduce albedo by accelerating snow sublimation, transformation of the snow structure, and snowmelt.[12] Increased snowmelt leads to earlier exposure of bare ice in the melt season, reducing albedo and further increasing annual melt volumes, in a positive feedback that is detrimental to glacier persistence.[25] At the same time, long-distance transport and deposition of light-absorbing particles can disproportionately darken glaciers compared to climate and have been recognized to reduce albedo in some regions of the Third Pole.[16,26–29] In addition, some glacier surface properties, including topography,[30] crystal/grain size,[31,32] and fine debris,[33] can also indirectly affect glacier albedo through interactions with local meteorology.[34]

Previous assessments have shown only slight temporal trends in glacier albedo across the Third Pole,[15,24,35] neglecting how interannual, seasonal, and altitudinal variability in albedo can mask these trends and shape long-term albedo changes. The seasonality of glacier albedo depends on the timing and intensity of snowfall; for example, snowfalls in spring can maintain high albedo until early summer. Albedo seasonality is therefore expected to vary from westerly-dominated to monsoon-dominated regions of the Third Pole (overall from west to southeast, respectively).[10,24] Altitudinal patterns of albedo may indicate the mechanisms of glacier change, such as snow-ice transitions,[36–39] debris emergence,[40,41] or deposition of light-absorbing particles from south Asia.[29] For example, expansion of bare ice and debris to a high altitude can lead to decreases of albedo, and dust and black carbon directly darken glacier/snow with a clear altitudinal pattern in the Indus Basin of the Third Pole.[29] Although trend analyses provide a primary basis for understanding near-term albedo change, understanding the temporal and spatial variability of albedo is necessary to disentangle the albedo sensitivity to drivers[10,14,42] and to project its future trajectories.

In this study, we characterize the interannual, seasonal, and altitudinal variability of albedo across the entire Third Pole from 2001 to 2020. We then exploit the interannual variability of glacier albedo to disentangle its sensitivity to key external drivers at the subregional scale and use these sensitivities to estimate glacier albedo change associated with climate projections. We also assess the broad impact of these glacier albedo projections on the "water tower of Asia." Our findings reveal that glacier albedo has declined with complex spatiotemporal patterns over 2001–2020 across the Third Pole, but interannual variability is also an important signal in this period. Glacier albedo variations show high sensitivity to air temperature and snow conditions, which suggests a continuous, much stronger decline in the 21st century, especially for the high warming scenario. These findings can be a scientific basis for policymakers and underline the urgency of action to mitigate climate warming in the Third Pole.

RESULTS AND DISCUSSION

Methods summary
We undertook four principal analyses (Figure S1). (1) We first retrieved daily glacier albedo values with an improved method[43] based on Moderate Resolution Imaging Spectroradiometer (MODIS) surface reflectance data (MOD09GA and MYD09GA) and then aggregated it to half-monthly, seasonal, and annual datasets. (2) We used the multi-year averages and linear trends to identify annual, seasonal, and altitudinal changes in annual glacier albedo during 2001–2020. (3) We determined the correlation of annual subregional albedos to eight potential drivers selected from ERA5-Land and MERRA-2 climate reanalysis and used the interannual variability to estimate the sensitivities of glacier albedo to each driver. (4) We constructed a multivariate linear regression model for glacier albedo in each subregion to estimate future albedo for three future climate scenarios. More details can be seen in the experimental procedures.

Subregional mean interannual albedo and trends
We obtain a complex spatial and temporal pattern of glacier albedo from MODIS. The mean annual albedo across the entire Third Pole is 0.532 ± 0.045, but it varies considerably between the regions (Figures 1A and 1B), with albedos in the westerly-dominated regions generally higher (0.52–0.58) than in the other subregions (0.48–0.51). Our results show that trends in glacier albedo are also highly variable in space (Figures 1A and 1C). Overall, glacier albedo shows a declining trend at a rate of -0.009 ± 0.008 dec^{-1} across the entire Third Pole. We find a small magnitude of change in the westerly-dominated regions (trend of -0.012 to $+0.005$ dec^{-1}), where two regions even show an albedo increase (Hindu Kush at $+0.006$ dec^{-1} and West Himalaya at $+0.005$ dec^{-1}, respectively). In contrast, the monsoon-dominated regions of the East Himalaya, Southeast Tibetan Plateau, and Hengduan Mountains show a moderate decrease in glacier albedo (-0.019 to -0.015 dec^{-1}). The most rapid decrease in glacier albedo occurs in the Inner Tibetan Plateau (-0.024 ± 0.013 dec^{-1}), which is the transition area of the westerly- to monsoon-dominated regions (Figures 1A and 1C). In the Karakoram, we find a lower mean albedo in the second decade than the first decade, providing further evidence of a recent reduction of the "Karakoram Anomaly."[5,9] In the West Kun Lun, a moderate glacier albedo decrease is associated with the transition from mass gain to loss,[9] demonstrating that the progressive decline in glacier persistence over the past 20 years indicated by the measurements at the Guliya Ice Cap[5,44] can be generalized to the entire Karakoram Anomaly region.

In addition to the complex spatial patterns of change, our results highlight that the observed annual trends remain weak relative to the interannual variability for most regions, as indicated by the trends' significance and standard deviation of the residuals of linear regression (σ_{resi}), which have been ignored in previous trend-based analyses (e.g., see Ming et al.,[24] Xiao et al.,[35] and Note S1 for more details). At $1° \times 1°$ and pixel-wide scales, >70% of the albedo trends are not significant at the 95% level (Figures 1C and S3), and >50% of the σ_{resi} exceeds the magnitude of the albedo change over the 20 years ($\Delta_{resi-trend} > 0$; Figures S2A and S4). Accordingly, 10 and eight subregions show these two phenomena, respectively (Figure 1A). These
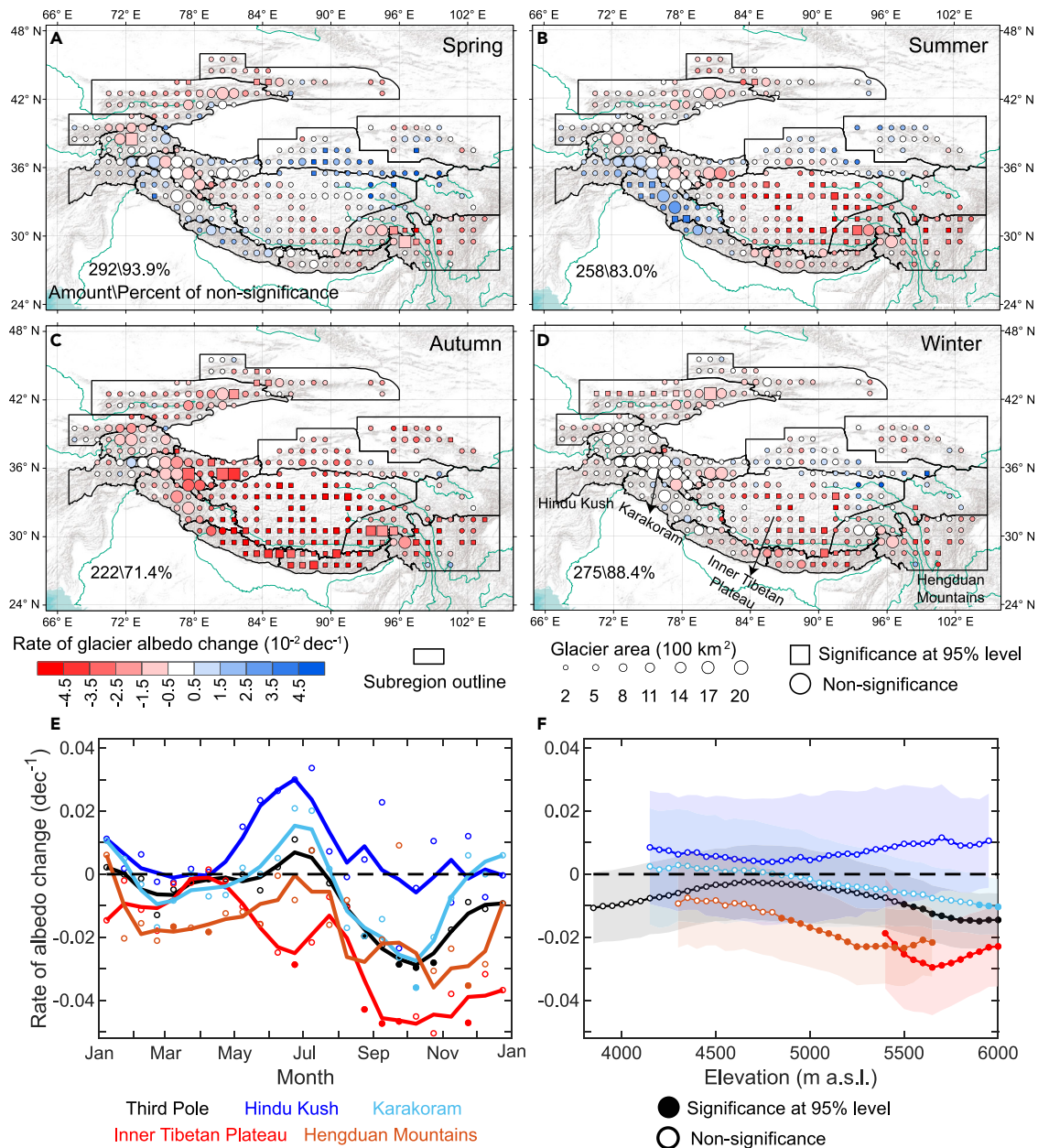
Figure 1. Glacier albedo and its decadal trend across the Third Pole for the period of 2001–2020, derived from MODIS surface reflectance data

(A) Annual albedo and its decadal trend in each subregion. The four numbers in each panel are the mean (Mean), the rate of annual albedo change (Trend, dec^{-1}), the standard deviation of the residual of the linear regression (σ_{resi}), and the coefficient of determination of the trend (R^2), respectively. The error bar shows the uncertainty of the annual albedo in each year (experimental procedures), and the shaded area shows the uncertainty of the trend at 95% confidence level. * and ** denote that the trend is significant at the 95% and 99% confidence levels, respectively. The geographical context of the entire Third Pole is shown in the center. Subregion boundaries indicate the second-order regions of RGI6.0.

(B and C) Maps of mean albedo (B) and rate of annual albedo change (C) in 1° × 1° grids. The number in the bottom left corner of (C) is the number/percentage of non-significant 1° × 1° grids.

findings emphasize that interannual variability is also an important signal in the glacier albedo time series in the Third Pole during the period of 2001–2020.

Seasonal and altitudinal patterns of glacier albedo

The pattern of seasonal albedo varies considerably across the Third Pole (Figure 2) and highlights the main mechanisms of glacier albedo change across the region. Glacier albedo shows

a stable or increasing trend in spring and early summer (Figures 2A and S5), especially in the westerly-dominated and winter-accumulating subregions, where glacier albedo follows a single-peak seasonal pattern (Figure S6). Albedo is partially decoupled from warming in these regions, as the winter accumulation is only marginally sensitive to warming or cooling. In contrast, a strong albedo decrease is observed in autumn (Figure 2C), when glacier albedo should be recovering to its

Figure 2. Seasonal and altitudinal patterns of the rate of glacier albedo change for the entire Third Pole and four subregions for 2001–2020
(A–D) Seasonal changes (spring, summer, autumn, and winter) on 1° × 1° grids. The number in the bottom left corner is the number/percentage of non-significant 1° × 1° grids.
(E) Rate of half-monthly glacier albedo changes in the entire Third Pole and the selected four subregions with distinct climate types. The solid line is the moving average of three half-month windows.
(F) Rate of altitudinal annual glacier albedo changes in the same regions as in (E). We display elevations between the 10th and 90th area percentiles because the extreme centiles have low numbers of observation. The shaded area indicates the uncertainty of the rate in each elevation bin.

maximum value. This decrease is more pronounced in the transitional and monsoonal subregions, such as the Inner Tibetan Plateau, the Southeast Tibetan Plateau, and the Hengduan Mountains, where glacier albedo has a second peak due to heavy snowfall in the post-monsoon season (Figure S6). Due to the high sensitivity of the solid precipitation ratio to air temperature in these regions, slight warming acts to significantly

decrease snowfall, leading to a pronounced change in autumn albedo and accelerated glacier mass loss.[25,45] Surprisingly, more precipitation (i.e., snowfall at high elevation) during the Indian monsoon and snow sublimation/aging due to dry air during the off-monsoon time act to balance the values of albedo between summer and winter in the Inner Tibetan Plateau and East Himalaya (Figures S7B, S9, and S10B).

Notably, the glacier albedo trends generally show a maximum decrease at higher elevations in westerly-dominated regions (Figures 2F and S11), especially in spring and autumn (Figure S12), possibly indicating an accelerated evolution of snow to firn in the accumulation zone. In monsoon-dominated and transitional regions, the maximum albedo decrease is observed in the middle elevations, likely due to the expansion of bare-ice ablation areas into high elevations (²F, S11, S12).[46] Close inspection also reveals contrasting seasonal albedo cycles at high and low elevations due to summer precipitation and phase controls (Figures S8–S10). However, as for the annual mean albedo, we also find strong signals of interannual variability in most seasonal and elevational albedos, as indicated by the high p value and large residual in these annual trends (Figures 2A–2D, S3, S4, and S13), reducing the confidence in these patterns as trends over the past 20 years. Indeed, glacier albedo fluctuates strongly due to frequent snow/ice changes on the glacier surface, especially when air temperature is near 0°C and snowfall occurs. Crucially, albedo is not only dependent on the meteorology in any given season but also on the surfaces inherited from previous seasons.

Sensitivity of glacier albedo to potential drivers

Because trends over the past 20 years are weak, they cannot be used to interpret past changes or extrapolate future trajectories. Instead, we exploit the strong interannual variability in glacier albedo (Figure 1A) to investigate its sensitivity to eight known drivers: air temperature, rainfall, snowfall, snow/rain ratio, snow cover, snow frequency, atmospheric dust, and atmospheric black carbon in the near-surface atmosphere. We aggregate annual time series for each driver from available reanalysis datasets and relate the interannual variability of glacier albedo to these drivers (Figure S14; experimental procedures). Our results highlight good correlations ($|R| > 0.6$) of glacier albedo with snow metrics and air temperature in most regions (Figure 3). The correlations of rainfall are low, with most $|R| < 0.4$, and vary between subregions due to its two-sided effect: i.e., heavy rainfall event can increase albedo in a short period by smoothing the glacier surface and washing out light-absorbing particles or fine debris,[33,47] thereby increasing albedo, whereas light rainfall can form a thin water layer on the glacier ice surface, thus decreasing albedo.[34] These correlations also vary in different seasons due to different dominant physical processes on the glacier surfaces (see details in Note S2). Atmospheric dust and black carbon show correlations only for the regions where their concentrations are very high due to nearby emission sources (Figure S15); glaciers around the Taklamakan desert are known to be affected by dust,[48,49] affecting the Pamir, Kunlun Mountains, and Qilian Mountains, while the Himalayan region is affected by black carbon according to our results ($|R| = 0.63$ to 0.78; Figure 3), as confirmed by local studies.[11,16] These results provide more spatially and temporally resolved details beyond the findings of Xiao et al.[35] and show that the effects of these drivers are also controlled by the local terrain, as in the Himalaya, where the difference in these drivers between northern and southern areas results in a distinctly different pattern of glacier albedo trend (Figure S16). In this region, glacier albedo on the southern area shows a stronger increase in the west but a stronger decrease in the east (see details in Note S3).

Glacier albedo shows a strong correlation with air temperature for most subregions of the Third Pole (Figure 3), including the areas with the highest albedo decline rates (Inner Tibetan Plateau, East Himalaya, and Hengduan Mountains). These occur preferentially in monsoonal areas undergoing rapid mass loss (-0.4 to -0.7 m w.e. a^{-1} [meter of water equivalent per year] for 2000–2019),[9] highlighting the sensitivity of glacier albedo and mass balance to air temperature for monsoonal maritime glaciers[45] due to its controls on precipitation phase and mass accumulation.[25] In westerly-dominated regions, such as the Karakoram and West Kun Lun, where glacier mass budgets have been close to neutral over the past 20 years (i.e., $< |0.08|$ m w.e. a^{-1}),[9] glacier albedo still correlates with annual air temperature but also with snowfall and snow cover. These regions experience high albedo during the short melt season moderated by the winter and spring snow cover (Figures S6, S8, and S10A), with strong implications for annual glacier mass balance.[44,50]

It is interesting that, in the westerly-affected northern ranges (Hissar Alay and Tien Shan), our results suggest a distinctly lower correlation of glacier albedo with air temperature ($|R| < 0.4$) than in other subregions with $|R| > 0.6$ (Figure 3). These regions also show reduced interannual variability and a moderate decrease in glacier albedo (-0.005 to -0.011 dec^{-1}; Figure 1A). The majority of glaciers in these regions are at lower elevations and are already losing mass at considerable rates,[9,18] consistent with their low annual albedos (<0.5). Our results indicate that albedos in summer mostly indicate bare ice with minimal snow cover, especially in the Hissar Alay and East Tien Shan (albedo < 0.3; Figure S6), resulting in less interannual variability and limited correlation with air temperature and limiting the potential future reduction of albedo. Furthermore, the snowfall and snow cover are close to zero in summer (Figure S17), which means they have a limited effect on (summer) glacier albedo.

Weak correlations in four seasons show that the effects of light-absorbing particles are complex and depend on meteorological drivers. In the Hindu Kush and West Himalaya, for example, deposition of light-absorbing particles has been found to reduce snow albedo by up to 3% at high elevations during March through August,[29] but our results show that glacier albedo during this period increased since 2000 due to increased snowfall and cooling (Figure S18), particularly affecting spring albedo (Figures 2A and 2E). However, the effects of light-absorbing particles are likely to become apparent with their exposure due to continued warming and snowmelt in the future. This result also emphasizes the need to consider the actual deposition of dust and black carbon and their interactions with the near-surface atmosphere to obtain a more robust assessment of the effects of light-absorbing particles on the cryosphere[26,29] (see Note S4 for additional exploration). Indeed, the evolution of glacier albedo is affected by complex interactions and feedback mechanisms between the glacier surface and the atmosphere. We have restricted our evaluation to impacts well documented in the literature and to analyses feasible with generally available datasets. A better understanding of the relative importance of different drivers of albedo change requires field observations and simulations that are beyond the scope of this study.

Glaciers will continually darken in the 21st century

As albedo plays a key role in the nonlinear sensitivity of mass balance to future climate change,[51] we estimated the response of
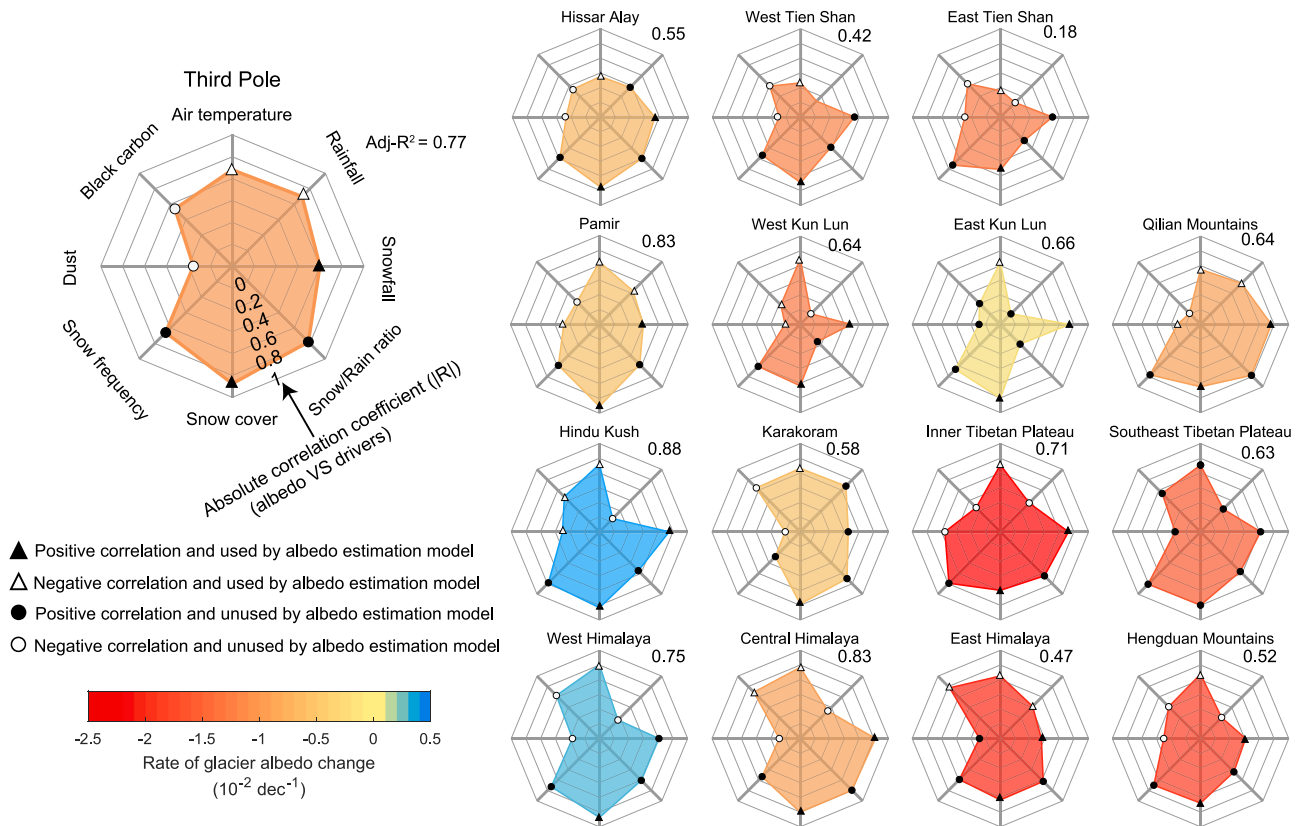
Figure 3. Correlation analysis between annual glacier albedo and eight potential drivers for the Third Pole and each subregion

The values are the absolute Pearson correlation coefficient (|R|); a solid triangle/circle represents positive correlation (R is positive), and a hollow triangle/circle represents negative correlation (R is negative). The triangle/circle indicates that the driver is used/unused by the albedo estimation model, and Adj-R^2 is the adjusted R^2 of the albedo estimation model (Table S3). The shaded area indicates the rate of annual glacier albedo change, which is consistent with Figure 1A. The subregional plots are positioned according to their locations in the Third Pole.

regional glacier albedo to future climate scenarios generated with 14 global climate models (GCMs) for three basic shared socioeconomic pathways (SSPs) combined with radiative forcing levels (SSP1–2.6, SSP2–4.5, and SSP5–8.5; Figures S19–S22). Glacier albedo is projected by applying a multivariate regression model in each subregion (experimental procedures; Table S3). Despite a variable range of the response across the Third Pole, the current albedo-driver sensitivity implies that annual glacier albedo will decrease by the end of the 21st century in all Third Pole regions and for all chosen SSP levels (Figure 4). If dust and black carbon continue their current trend (Figure S23), the mean annual glacier albedo is limited to a 2.9% ± 2.5% decrease (percent of the mean albedo in 2001–2020) for the entire Third Pole under SSP1-2.6 at the end of the 21st century but will undergo stronger declines for SSP2–4.5 (6.4% ± 3.2%) and SSP5–8.5 (12.5% ± 5.7%). Such extreme albedo declines under SSP5-8.5 lead to a mean annual Third Pole glacier albedo value of 0.45, corresponding to exposed glacier ice for most of the glacier area and most of the year. In contrast, under SSP1–2.6, most subregions would experience annual glacier albedos above 0.45 by the end of the 21st century, and the annual glacier albedo in the Third Pole would stabilize above 0.5. Based on initial estimates, glacier albedo reduction under SSP5–8.5 could contribute to a mean mass loss increase of 170% and water

runoff increase of 70% during 2015–2100 over the entire Third Pole compared to the past 20 years (Figures S24 and S25).

Under these scenarios, the subregions largely differ in their expected albedo response and in associated glacier mass balance, indicating that the imbalance of the water tower of Asia is likely to persist and even intensify in the 21st century.[5] In general, our projections indicate strong reductions in glacier albedo in the transitional (Inner Tibetan Plateau) and monsoon-dominated regions (East Himalaya, Southeast Tibetan Plateau, and Hengduan Mountains), where the decreases in the mean annual glacier albedo may exceed 20% to reach values below 0.4 at the end of the 21st century under SSP5–8.5 (Figure 4), which could be explained by an increase in net shortwave radiation of about 22–42 W m^{-2} in the melt season and an increase in annual glacier mass loss of 1.04–1.82 m w.e. a^{-1} (Figure S24). Interestingly, the glacier albedo reduction in these regions is distinctly slower after 2080, which could be related to changes in the liquid monsoon precipitation ratio. Due to continuous warming and the phase change of precipitation from solid to liquid in the post-monsoon season, the double-peak pattern in glacier albedo in these regions could change to a single-peak pattern (Figure S6), which has less potential for further albedo decline and, thus, shows a slow rate of decrease after 2080. In the East Tien Shan, annual glacier albedo shows less reduction in response to future climate
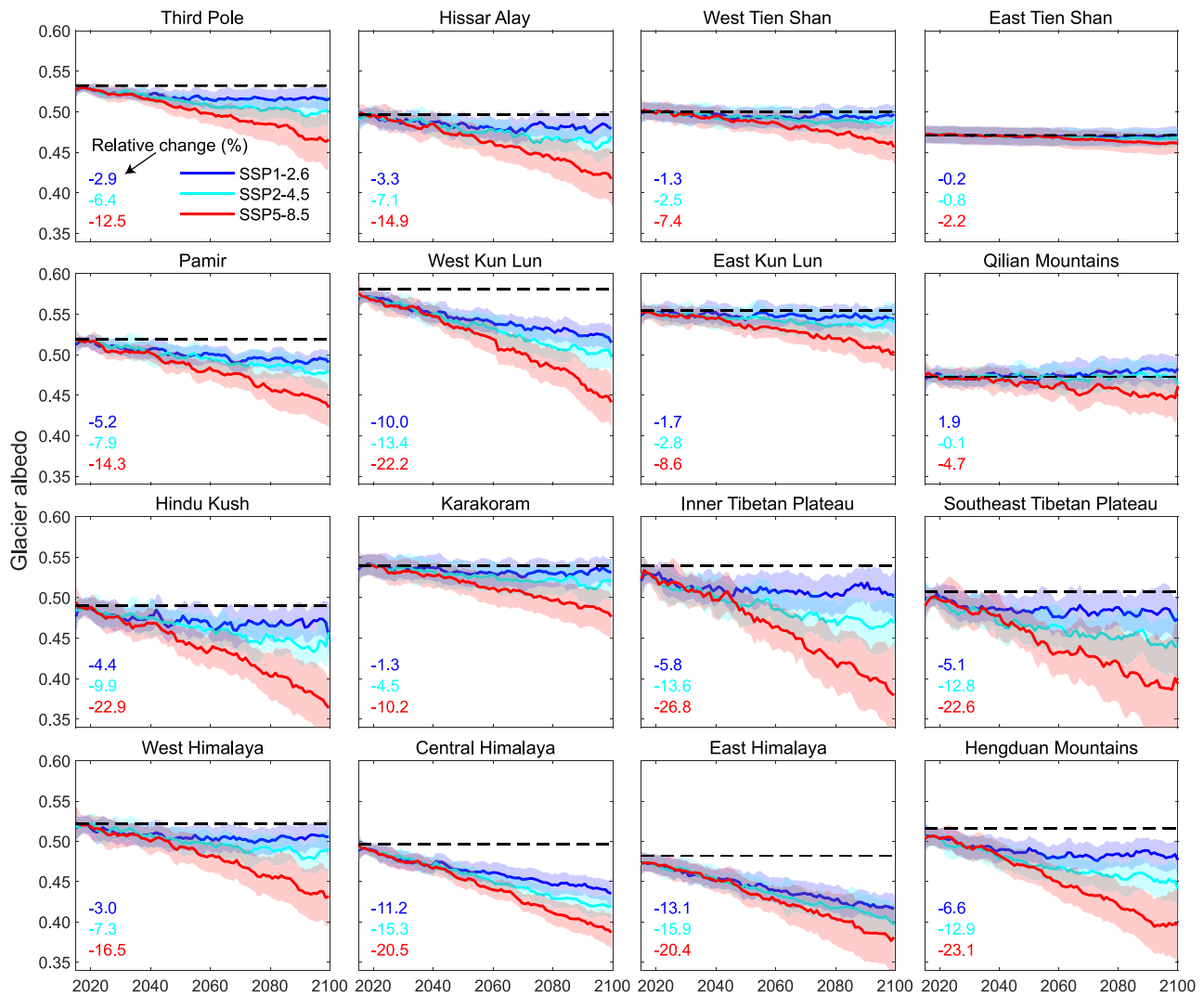
Figure 4. Projected changes in annual glacier albedo in response to three future climate scenarios associated with the current linear trend in dust and black carbon concentration

The solid line is the median of the ensemble glacier albedos estimated by the 14 GCMs, smoothed with a moving average over a 5-year window. The shaded area indicates the uncertainty in the glacier albedo projection ($\sigma_{projection}$; Equation 9; experimental procedures). The number is the relative change (%) in mean glacier albedo during the last decade of the 21st century (2091–2100) compared with the first two decades (2001–2020, black dashed line). More details in dust and black carbon concentration can be seen in the section of glacier albedo projections under experimental procedures and in Figure S23.

warming, resulting from reduced sensitivity to warming due to its already low albedos in the absence of summer snow (Figure 3) and the projected increases of total precipitation and a slower future decline of snowfall under a warmer climate in that region (Figure S21). We also recommend more focused study of the snowfall and albedo dynamics in this region. The large differences in albedo decline under SSP1–2.6 and SSP5–8.5 highlight the potential for strong and immediate global climate change mitigation to prevent further regional glacier albedo decline and glacier mass balance feedback.

In addition, we also find that the albedo decline and glacier mass loss could be mitigated to some extent by reducing the atmospheric black carbon in the Central and East Himalaya (Figure S26). If atmospheric black carbon is to keep following the

current (2001–2020) linear trend, this would result in an albedo reduction of about 0.04 and a glacier mass loss increase of about 0.5 m w.e. a^{-1} at the end of 21st century across these local regions compared to a scenario where black carbon remains at the current level. In the best case with zero black carbon, increasing albedo could lead to a mass increase in the Himalayas even under the worst climate scenario (SSP5–8.5). This sensitivity experiment highlights the urgency of actions to reduce atmospheric black carbon in south Asia.

According to the good correlation between glacier albedo and mass balance across the Third Pole (Figure S27) and the important contribution of albedo change to the total future mass balance (Figure S24), this extrapolation of the contemporary glacier albedo response to end-of-century conditions highlights the

importance of accounting for glacier albedo change in projections of glacier change.[52,53] However, this response is complicated by processes such as increased rates of snow metamorphism, glacier surface debris, cryoconite, and changes in firn water content, each of which may contribute to further nonlinearity in the response of glacier albedo to climate change.[12,54] In this regard, physical glacier models describing ice and snow albedo dynamics[55] and melt consequences[52,56,57] are necessary to obtain a more accurate response and feedback of glacier albedo to near-surface atmospheric conditions under projected climate change. This approach, however, requires considerable computational resources to study large regions. The spatiotemporal albedo data derived with our improved retrieval method are an important support for the development and calibration of such models at interannual and decadal timescales.[53]

Conclusions

We have shown that glacier albedo and its interannual variability, trend, and altitudinal distribution exhibit large spatiotemporal differences across the Third Pole during the first two decades of the 21st century. Interannual variability in particular belies the trends in the majority of the Third Pole. We identify air temperature and solid precipitation as the main potential drivers of the spatial and temporal variability in the glacier albedo. The interplay of these two driving variables is complex and highly variable spatially across different climatic regimes of the Third Pole. We then use this new understanding of the effects of drivers on glacier albedo to estimate future changes in glacier albedo through the end of the century. We demonstrate that strong decreases in glacier albedo are expected in most subregions of the Third Pole for the worst socio-economic scenarios, with particularly remarkable decreases in the Inner Tibetan Plateau, Southeast Tibetan Plateau, East Himalaya, and Hengduan Mountains, where the SSP5–8.5 scenario implies a region-wide decrease in glacier albedo of 20% at the end of the 21st century, resulting in an annual net shortwave radiation increase of about 22–42 W m^{-2} in the melt season and glacier mass loss of 1.04–1.82 m w.e. a^{-1}. This indicates that additional energy absorption will play an important role in accelerating the demise of glaciers across the region. However, our results also show the relative insensitivity of glacier albedo to projected climate change in westerly-dominated regions. Our results thus provide a picture of future changes for a key nonlinear element of the response of glacier-climate system and show that the response of glacier albedo to precipitation and temperature changes is an important but neglected mechanism of the nonlinear sensitivity of glaciers to future climate change, highlighting the importance of accounting for glacier albedo as a feedback mechanism in future projections of glacier change. Our results also highlight the importance of reduction measures for atmospheric black carbon to reduce glacier mass loss, especially in the Himalayas.

EXPERIMENTAL PROCEDURES

Glacier classification for each MODIS pixel

The purpose of our study is to investigate changes in glacier albedo, we therefore classify MODIS pixels by surface type and then keep only clean-ice/snow pixels. As Figure S28 shows, we rasterize the glacier outlines from the Randolph Glacier Inventory v.6.0 (RGI6.0) at a 30-m resolution and then aggregate this raster to the MODIS pixel footprints (500 × 500 m)

to estimate the glacier fractional abundance within each MODIS pixel. Only MODIS pixels with >50% glacier fractional abundance are classified as glacier pixels. Although not free from problems, the inventory is suitable for regional and global studies[58] and has been widely used by the glaciological community.[9,59] Similarly, we estimate the on-glacier debris fractional abundance using the debris cover extents from Scherler et al.[60] and keep clean-ice/snow pixels (those without surface debris) by applying the same 50% threshold to glacier pixels. In this study, both errors in the RGI6.0 dataset and in the glacier classification method can introduce mixed MODIS pixels, resulting in a surface reflectance that combines signals from mixed targets. These errors may affect absolute glacier albedo values but are unlikely to affect the spatiotemporal variability of albedo (the main result of this study), as indicated by our assessment of the effect of mixed MODIS pixels (see Note S4 for more details).

Improved MODIS glacier albedo
Albedo retrieval

We use the method developed by Ren et al.[43] to retrieve the daily glacier albedo (broadband shortwave albedo) with MODIS surface reflectance (MYD09GA and MOD09GA) for all cloud-free MODIS pixels (hereafter, we refer to this product as improved MODIS albedo to distinguish it from the standard MODIS albedo product (MCD43A3). By applying an updated anisotropy correction on snow and ice surfaces, this method can retrieve both snow and ice albedo, respectively, and gives a better agreement with *in situ* albedo measurements and better temporal coverage than MCD43A3.[43] This method distinguishes between the albedo of glacier ice and of snow, in contrast to the standard MODIS snow albedo product (MOD10A1 and MYD10A1).[61] This allows the data to better represent the spatiotemporal variability of glacier albedo. The method includes three steps[43,62]: (1) Topography correction. Since terrain modifies the orientation of a target relatively to the satellite and sun, two functions based on terrain factors were used to correct this relative position.[63] Terrain factors, including slope and aspect, were retrieved from the Advanced Land Observing Satellite World 3D-30m Digital Surface Model,[64] and the sun and view zenith and azimuth were read from the MODIS ancillary data at 1-km spatial resolution. (2) Narrowband albedo retrieval by applying an anisotropic correction. The anisotropic factor for each band was determined by the corrected orientation of the target relative to the sun and satellite in the first step and then applied to convert bi-conical surface reflectance to narrowband albedo. (3) Broadband albedo estimated by applying empirical equations. Two different equations were used to convert narrowband to broadband albedo of the ice and snow surface (α_{ice} and α_{snow}), according to Liang[65] and Stroeve et al.,[66] respectively:

$$\alpha_{ice} = 0.160b_1 + 0.291b_2 + 0.243b_3 + 0.116b_4 + 0.112b_5 + 0.081b_7 - 0.0015 \text{ and}$$

(Equation 1)

$$\alpha_{snow} = 0.1574b_1 + 0.2789b_2 + 0.3829b_3 + 0.1131b_5 + 0.0694b_7 - 0.0093,$$

(Equation 2)

where b_i (i = 1, 2, …, 7) represents the estimated narrowband albedo in the i-th MODIS band in the second step. Snow on the glacier surfaces was detected by normalized difference snow index > 0.4.

Daily albedo was then generated using broadband albedos from both Terra and Aqua satellites and aggregated to half-monthly values by determining the average of all valid retrievals within each half-month period. These products were generated in Google Earth Engine, which allowed the processing of this very large dataset. Remaining gaps for a given half-month time step were spatially interpolated over the eight nearest-neighbor pixels in two iterations. After this spatial interpolation, the percentage of valid data of the half-monthly products improved from 94% to 99% overall and especially in winter (from 85% to 97%), which is sufficient to characterize the glacier albedo change across the area. We then determined seasonal and annual glacier albedos by averaging the half-monthly albedo for each calendar season.

Uncertainty of the retrieved albedo

The region-wide uncertainty accounts for temporal (half-month, seasonal) and spatial (each subregion) uncertainty, and it is estimated in two steps.

(1) First, we determine the temporal uncertainty for each pixel ($\sigma_{half\text{-}month\_pixel}$). It is estimated by assuming that the daily albedos are independent during a half-month period[67]:

$$\sigma_{half\text{-}month\_pixel} = \frac{\sigma_{pixel}}{\sqrt{N}}, N \geq 2, \qquad \text{(Equation 3)}$$

where σ_{pixel} is the standard deviation of valid daily albedos in each half-month interval, and N is their number. The seasonal and annual uncertainties of the pixel albedo ($\sigma_{period-pixel}$) are calculated as follows:

$$\sigma_{period\_pixel} = \sqrt{\overline{\sigma_{half\text{-}month\_pixel}}^2 + \sigma\sigma_{half\text{-}month\_pixel}^2}, \qquad \text{(Equation 4)}$$

where $\overline{\sigma_{half\text{-}month\_pixel}}$ is the average of $\sigma_{half\text{-}month\_pixel}$ in a given period, and $\sigma\sigma_{half\text{-}month\_pixel}$ is the standard deviation.

(2) We then aggregate the resulting pixel-wise uncertainties at the regional scale. Similarly, we estimate the regional uncertainty (σ_{period}) as the average ($\overline{\sigma_{period\_pixel}}$) and standard deviation ($\sigma\sigma_{period\_pixel}$) of uncertainty of all pixels in each subregion:

$$\sigma_{period} = \sqrt{\overline{\sigma_{period\_pixel}}^2 + \sigma\sigma_{period\_pixel}^2}. \qquad \text{(Equation 5)}$$

Trend of glacier albedo

All albedo trends were estimated by applying linear regression to observations at both subregional and $1° \times 1°$ scales, and their uncertainties were provided by the 95% confidence interval of the trends. Prior to trend estimation, pixel-wise albedos were averaged over each subregion or each $1° \times 1°$ grid. To distinguish whether albedo is dominated by trend or interannual variability, two indices are used: the p value of the trend and $\Delta_{residual\text{-}trend}$ (Figure S2), which is the difference between the standard deviation of the residual of the linear regression ($\sigma_{residual}$) and the magnitude of linear change over the past 20 years:

$$\Delta_{residual\text{-}trend} = \sigma_{residual} - |20 * trend|, \qquad \text{(Equation 6)}$$

where $trend$ is the rate of linear change. Albedo is more likely to be dominated by interannual variability when $p > 0.05$ or $\Delta_{residual\text{-}trend} > 0$.

Driving factor analysis

Meteorological conditions can affect glacier albedo by altering the evolution of glacier surface properties,[10,11,33,35,36] while light-absorbing particles can directly darken glacier surfaces.[15,16,29] Some glacier surface properties, such as microtopography or crystal/grain size[31] and fine debris[33] are not considered due to their indirect effects and the difficulty in quantifying them.[34] We expect these factors to be the main drivers of temporal variability of glacier albedo and test their association with measured albedo changes. We consider six atmospheric forcing variables (i.e., air temperature, rainfall, snowfall, snow/rain ratio, snow cover, and snow frequency) derived from the ERA5-Land reanalysis data with a spatial resolution of $0.1° \times 0.1°$ ($\sim$9 km)[68] and the concentrations of two major light-absorbing particles in the near-surface atmosphere; i.e., atmospheric dust and atmospheric black carbon from MERRA-2 reanalysis data[69] with a spatial resolution of $0.5° \times 0.625°$. Only the pixels overlying glacier are used for this analysis to ensure they reflect atmospheric conditions in the vicinity of glaciers. According to previous studies (e.g., Wang et al.[70]), ERA5-Land data are subject to some seasonal biases, but ERA5 and ERA5-Land are nonetheless widely used in the assessment of meteorological conditions in glacierized regions of the Third Pole.[9,71–74] Moreover, similar patterns in temporal variability derived by ERA5-Land and MODIS albedo (Figure S29) indicate that ERA5-Land is a way to characterize atmospheric forcing in an area partly occupied by glaciers. However, rather large differences also indicate that ERA5-Land albedo is unreliable to directly quantify the spatiotemporal change of mountain glacier albedo, which is one of the motivations of this study. We assess the correlation of albedo with each driver

using the Pearson correlation coefficient (R) for each subregion (Figure 3). We first aggregate these drivers by averaging all overlying glacier pixels in each subregion at the annual scale and then assess their correlations with albedo. In addition, to evaluate the orographic effect of the Himalayan crest on the albedo patterns, we manually delineate its ridge line in Google Earth and use a 50-km buffer to distinguish the north and north slopes of the range (Figure S16A).

Glacier albedo estimation model

In most glaciological and hydrological models, albedo is estimated from climatic factors (e.g., air temperature, snow, and relative humidity).[75,76] Similarly, we establish a multivariate linear regression model to estimate annual glacier albedo for each subregion using the observed sensitivities of glacier albedo to the potential drivers. Our selection of potential drivers of changes in glacier albedo is mainly based on causality established in the literature.[10,11,15,16,29,35,36] The role of our multivariable linear regression analysis is limited to the estimation of partial sensitivities once the potential drivers have been identified and their role in the observed variability of albedo has been documented by literature. The model is

$$a(t) = B_0 + \sum_{i=1}^{6} B_i X_i(t), \qquad \text{(Equation 7)}$$

where t denotes the year, X_i ($i = 1, 2, …, 6$) are the six candidate drivers mentioned above except snow/rain ratio and snow frequency, B_0 is a constant, and B_i ($i = 1, 2, …, 6$) are the multivariate regression coefficients simultaneously estimated using observations from 2001–2020. Snow frequency is discarded because of its unavailability in CMIP6 data, while snow/rain ratio is discarded because it needs to be further calculated from rainfall and snowfall, which could carry more uncertainty. Before estimating this multi-linear regression, it is necessary to assess the independence of these six potential drivers; we therefore conduct a correlation analysis (Figure S30). The results show that Pearson correlation coefficients between snow conditions (snowfall and snow cover) and air temperature range from -0.1 to -0.9, indicating that air temperature only partially influences snow conditions. Indeed, within the ERA5-Land model chain, snowfall and snow cover depend not only on temperature but also on other variables, such as cloud, humidity, and snow energy budget.[68] We follow a two-step approach to include only significant drivers. (1) Since temperature and snow cover are the main drivers in almost all subregions, we first build an initial regression model using only these two drivers. (2) We iteratively add the remaining drivers to the model, starting with the highest R value (Figure 3), keeping them only if the adjusted R^2 (Adj-R^2) improved by more than 5%.[77] The evaluation of the estimated relationships shows that the regression performs well across the entire Third Pole, with Adj-R^2 = 0.77, $p < 0.01$, and root-mean-square error (RMSE) = 0.005. 10 of the 16 regressions have Adj-R^2 > 0.6, 15 with $p < 0.05$, and 7 with RMSE < 0.01 (Table S3), indicating that our approach can estimate glacier albedo well in most subregions. Especially, a consistency test also shows that the glacier albedo over the entire Third Pole derived by the multi-linear regression model is slightly higher than that estimated by area-weighted average with 15 subregional glacier albedos, and their temporal evolutions are very similar as well (Figure S31).

Glacier albedo projections

In our effort to estimate glacier albedo response to future climate, we rely on current sensitivities of glacier albedo to the drivers remaining stable as the climate warms, although the interaction between our presumed drivers and glacier surface albedo is complex. It should be noted that these sensitivities may change in different meteorological conditions.[12,76] Similar assumptions regarding the stability of the sensitivity of mass balance to climate have been applied in projections by regional-scale glacier models.[59,78] The cross-validation experiment shows that the glacier albedo in 2011–2020 can be well estimated using the relationships established for 2001–2010 (see Note S4 for more details; Figure S32), indicating the reliability of this assumption. The multivariate model was applied from 2015 to 2100, driven by the 14 GCMs from the Scenario Model Intercomparison Project (ScenarioMIP) of the Climate Model Intercomparison Project Phase 6 (CMIP6).[79] CMIP6 includes better-constrained climate forcing and aerosol emissions by coupling more physical processes in different earth subsystems.[80] Because there is

large disagreement regarding atmospheric dust and black carbon due to limitations in the available GCMs, we instead assume that no action is taken to mitigate the trend of dust and black carbon emissions; i.e., that the annual dust and black carbon in the 21st century are estimated using the same linear trends derived for 2001–2020 (Figure S23) and used to estimate albedo in the future (Figure 4). To assess the impact of mitigation of black carbon emissions on glacier albedo, we compare the albedos under five scenarios for 21st century black carbon changes: extrapolation of the current linear trend as described, extension of the current state (average during 2001–2020), and decreases of 10%, 50%, and 100% during 2015–2100 relative to the current state (Figures S22A–S22C). ScenarioMIP provides multi-model climate projections for five SSPs and seven radiative forcing levels. We select the 14 GCMs that include four climate forcings for three baseline scenarios (SSP1–2.6, SSP2–4.5, and SSP5–8.5; Table S2; Figures S19–S22). All selected GCM data belong to the "r1i1p1f1" ensemble member, which is widely used for impact assessment of future climate.[78,81,82] For the reanalysis data, only the pixels intersected with glacier in GCMs are used for future albedo estimation. Since there are large differences between the GCMs and the reanalysis data, we correct the GCMs against ERA5-Land for climatic factors in the overlap period 2015–2020 by

$$GCM_{correct} = GCM_{raw} - (GCM_{overlap} - Reference_{overlap}), \quad \text{(Equation 8)}$$

where $GCM_{correct}$ and GCM_{raw} are the corrected and raw GCM, $GCM_{overlap}$ is the mean value of the raw GCM data from 2015 to 2020, and $Reference_{overlap}$ is the mean value of ERA5-Land in 2015–2020. This is analogous to the "delta" method for the forcing of our multivariate model and allows us to estimate the albedo expected for future climatic conditions given the current albedo sensitivity to climate variability. We then estimate the uncertainty of the projected annual glacier albedo ($\sigma_{projection}(t)$) as the quadratic sum of the RMSE of the albedo estimation model ($RMSE_{model}$) and the standard deviation of the annual glacier albedos in the GCM composite ($Std_{GCMs}(t)$):

$$\sigma_{projection}(t) = \sqrt{RMSE_{model}^2 + Std_{GCMs}(t)^2}. \quad \text{(Equation 9)}$$

Impact of projected glacier albedo on mass balance
Due to the direct control of the net shortwave radiation, glacier albedo can affect glacier melt, sublimation, and evapotranspiration. To assess the relative impact of glacier albedo changes on glacier melt in different scenarios and subregions, given the large spatial scales considered, we assume that changes in the net shortwave radiation caused by albedo changes during the melt season directly influence glacier melt, i.e., we estimated the impact on glacier mass balance by assuming that all additional melt-season radiative energy would be used for melt. Moreover, we also make the following two conservative assumptions to estimate the resulting mass loss in future climate scenarios based on our annual albedo estimates: (1) the number of days during the melt season are stable (but they are likely to increase), and (2) albedo change in melt season is the same as the annual albedo changes (albedo changes are most pronounced during the melt season). As a result, we can write the change in net shortwave energy (NSR_{add}) caused by changes in albedo as

$$NSR_{add} = DSR * (a_{reference} - a_{future}) * MD, \quad \text{(Equation 10)}$$

where DSR is the mean daily downward shortwave energy in melt season during 2001–2020, $a_{reference}$ is the mean area-averaged glacier albedo during 2001–2020, a_{future} is the annual area-averaged albedo in a given future climate scenario, and MD is the number of days of glacier melt. DSR is calculated by ERA5-Land reanalysis data, and MD is mean melting days during 2017–2020 according to the study of Scher et al.,[83] and we set MD in the Tien Shan and Hissar Alay, which were not covered in the study, to May–September, in agreement with nearby regions. The area-averaged glacier mass balance caused by albedo change (MB in m w.e. a^{-1}) can then be obtained from the changes in net shortwave energy:

$$MB = -\frac{NSR_{add}}{Q_{melt} * \rho_w}, \quad \text{(Equation 11)}$$

where Q_{melt} is the latent heat of melt per unit mass of ice (i.e., 336,000 J kg^{-1}), and ρ_w is the density of water (i.e., 1,000 kg m^{-3}). The uncertainties of additional net shortwave energy (σ_{NSR_add}) and additional mass balance (σ_{MB_change}) are estimated based on the obtained uncertainty of future albedo ($\sigma_{projection}(t)$; Equation 9) coupled with Equations 10 and 11:

$$\sigma_{NSR\_add} = DSR * \sigma_{projection}(t) * MD \quad \text{(Equation 12)}$$

$$\sigma_{MB\_change} = \frac{\sigma_{NSR\_add}}{Q_{melt} * \rho_w} \quad \text{(Equation 13)}$$

As glacier albedo, we also assess the impact of the mitigation of black carbon emissions on glacier mass balance (Figures S26D–S26F). To quantify the impact of albedo change on water availability, we assume that (1) all additional net shortwave radiation would be used to melt snow and ice and (2) no meltwater would be retained by the glacier or by glacial lakes. This means that all meltwater would freely flow downstream and contribute to the water yield of high-elevation catchments. We then translate the area-averaged glacier mass balance to volume change to estimate the annual water runoff (W_{runoff}) caused by glacier albedo change (Figure S25):

$$W_{runoff} = MB * Area, \quad \text{(Equation 14)}$$

where $Area$ is the glacier area in each year during 2015–2100.[84] Since this study only provides glacier area in three years (2040, 2070, and 2100), we estimate annual glacier area by assuming that glacier retreats with a linear change in these periods.

Overall, this estimation may be conservative. Although the downward shortwave energy has slightly decreased (-1.4 W m^{-2} dec^{-1}) in the past 20 years, the snow melt season has significantly extended by 4–12 days dec^{-1},[85] and albedo in melt season (May–September) indeed decreases faster than annual albedo (Figure S5). This means that the added net shortwave energy is more than our estimation, i.e., the true mass loss and glacier runoff due to albedo change could be more in the future.

AUTHOR CONTRIBUTIONS

Conceptualization, S.R., L.J., E.S.M., M.M., and F.P.; methodology, S.R., E.S.M., L.J., and M.M.; resources, L.J., M.M., F.P., and T.Y.; visualization, S.R.; project administration and supervision, L.J., M.M., F.P., and T.Y.; writing – original draft, S.R.; writing – review and editing, all authors.

DECLARATION OF INTERESTS

The authors declare no competing interests.

SUPPLEMENTAL INFORMATION

REFERENCES

1. Yao, T., Thompson, L., Yang, W., Yu, W., Gao, Y., Guo, X., Yang, X., Duan, K., Zhao, H., Xu, B., et al. (2012). Different glacier status with atmospheric circulations in Tibetan Plateau and surroundings. Nat. Clim. Chang. *2*, 663–667. https://doi.org/10.1038/nclimate1580.

2. Bolch, T., Shea, J.M., Liu, S., Azam, F.M., Gao, Y., Gruber, S., Immerzeel, W.W., Kulkarni, A., Li, H., Tahir, A.A., et al. (2019). Status and Change of the Cryosphere in the Extended Hindu Kush Himalaya Region. In The Hindu Kush Himalaya Assessment: Mountains, Climate Change, Sustainability and People, pp. 209–255. https://doi.org/10.1007/978-3-319-92288-1_7.

3. Pritchard, H.D. (2019). Asia's shrinking glaciers protect large populations from drought stress. Nature *569*, 649–654. https://doi.org/10.1038/s41586-019-1240-1.

4. Immerzeel, W.W., Lutz, A.F., Andrade, M., Bahl, A., Biemans, H., Bolch, T., Hyde, S., Brumby, S., Davies, B.J., Elmore, A.C., et al. (2020). Importance and vulnerability of the world's water towers. Nature *577*, 364–369. https://doi.org/10.1038/s41586-019-1822-y.

5. Yao, T., Bolch, T., Chen, D., Gao, J., Immerzeel, W., Piao, S., Su, F., Thompson, L., Wada, Y., Wang, L., et al. (2022). The imbalance of the Asian water tower. Nat. Rev. Earth Environ. *3*, 618–632. https://doi.org/10.1038/s43017-022-00299-4.

6. Ragettli, S., Bolch, T., and Pellicciotti, F. (2016). Heterogeneous glacier thinning patterns over the last 40 years in Langtang Himal, Nepal. Cryosphere *10*, 2075–2097. https://doi.org/10.5194/tc-10-2075-2016.

7. Zemp, M., Huss, M., Thibert, E., Eckert, N., McNabb, R., Huber, J., Barandun, M., Machguth, H., Nussbaumer, S.U., Gärtner-Roer, I., et al. (2019). Global glacier mass changes and their contributions to sea-level rise from 1961 to 2016. Nature *568*, 382–386. https://doi.org/10.1038/s41586-019-1071-0.

8. Maurer, J.M., Schaefer, J.M., Rupper, S., and Corley, A. (2019). Acceleration of ice loss across the Himalayas over the past 40 years. Sci. Adv. *5*, eaav7266. https://doi.org/10.1126/sciadv.aav7266.

9. Hugonnet, R., McNabb, R., Berthier, E., Menounos, B., Nuth, C., Girod, L., Farinotti, D., Huss, M., Dussaillant, I., Brun, F., and Kääb, A. (2021). Accelerated global glacier mass loss in the early twenty-first century. Nature *592*, 726–731. https://doi.org/10.1038/s41586-021-03436-z.

10. Ming, J., Du, Z., Xiao, C., Xu, X., and Zhang, D. (2012). Darkening of the mid-Himalaya glaciers since 2000 and the potential causes. Environ. Res. Lett. *7*, 14021. https://doi.org/10.1088/1748-9326/7/1/014021.

11. Ming, J., Xiao, C., Du, Z., and Yang, X. (2013). An overview of black carbon deposition in High Asia glaciers and its impacts on radiation balance. Adv. Water Resour. *55*, 80–87. https://doi.org/10.1016/j.advwatres.2012.05.015.

12. Johnson, E., and Rupper, S. (2020). An Examination of Physical Processes That Trigger the Albedo-Feedback on Glacier Surfaces and Implications for Regional Glacier Mass Balance Across High Mountain Asia. Front. Earth Sci. (Lausanne) *8*, 1–18. https://doi.org/10.3389/feart.2020.00129.

13. Fugazza, D., Senese, A., Azzoni, R.S., Maugeri, M., Maragno, D., and Diolaiuti, G.A. (2019). New evidence of glacier darkening in the Ortles-Cevedale group from Landsat observations. Glob. Planet. Change *178*, 35–45. https://doi.org/10.1016/j.gloplacha.2019.04.014.

14. Shaw, T.E., Ulloa, G., Farías-Barahona, D., Fernandez, R., Lattus, J.M., and McPhee, J. (2021). Glacier albedo reduction and drought effects in the extratropical Andes, 1986–2020. J. Glaciol. *67*, 158–169. https://doi.org/10.1017/jog.2020.102.

15. Zhang, Y., Gao, T., Kang, S., Shangguan, D., and Luo, X. (2021). Albedo reduction as an important driver for glacier melting in Tibetan Plateau and its surrounding areas. Earth. Sci. Rev. *220*, 103735. https://doi.org/10.1016/j.earscirev.2021.103735.

16. Kang, S., Zhang, Y., Qian, Y., and Wang, H. (2020). A review of black carbon in snow and ice and its impact on the cryosphere. Earth. Sci. Rev. *210*, 103346. https://doi.org/10.1016/j.earscirev.2020.103346.

17. Tang, S., Vlug, A., Piao, S., Li, F., Wang, T., Krinner, G., Li, L.Z.X., Wang, X., Wu, G., Li, Y., et al. (2023). Regional and tele-connected impacts of the Tibetan Plateau surface darkening. Nat. Commun. *14*, 32. https://doi.org/10.1038/s41467-022-35672-w.

18. Brun, F., Berthier, E., Wagnon, P., Kääb, A., and Treichler, D. (2017). A spatially resolved estimate of High Mountain Asia glacier mass balances from 2000 to 2016. Nat. Geosci. *10*, 668–673. https://doi.org/10.1038/ngeo2999.

19. Zhang, G., Kang, S., Cuo, L., and Qu, B. (2016). Modeling hydrological process in a glacier basin on the central Tibetan Plateau with a distributed hydrology soil vegetation model. J. Geophys. Res. *121*, 9521–9539. https://doi.org/10.1002/2016JD025434.

20. Yang, W., Guo, X., Yao, T., Yang, K., Zhao, L., Li, S., and Zhu, M. (2011). Summertime surface energy budget and ablation modeling in the ablation zone of a maritime Tibetan glacier. J. Geophys. Res. *116*, 141166–D14211. https://doi.org/10.1029/2010JD015183.

21. Nicholson, L.I., Prinz, R., Mölg, T., and Kaser, G. (2013). Micrometeorological conditions and surface mass and energy fluxes on Lewis Glacier, Mt Kenya, in relation to other tropical glaciers. Cryosphere *7*, 1205–1225. https://doi.org/10.5194/tc-7-1205-2013.

22. Fugger, S., Fyffe, C.L., Fatichi, S., Miles, E., McCarthy, M., Shaw, T.E., Ding, B., Yang, W., Wagnon, P., Immerzeel, W., et al. (2022). Understanding monsoon controls on the energy and mass balance of glaciers in the Central and Eastern Himalaya. Cryosphere *16*, 1631–1652. https://doi.org/10.5194/tc-16-1631-2022.

23. Mortimer, C.A., Sharp, M., and Van Wychen, W. (2018). Influence of recent warming and ice dynamics on glacier surface elevations in the Canadian High Arctic, 1995-2014. J. Glaciol. *64*, 450–464. https://doi.org/10.1017/jog.2018.37.

24. Ming, J., Wang, Y., Du, Z., Zhang, T., Guo, W., Xiao, C., Xu, X., Ding, M., Zhang, D., and Yang, W. (2015). Widespread albedo decreasing and induced melting of Himalayan snow and ice in the early 21st century. PLoS One *10*, e0126235. https://doi.org/10.1371/journal.pone.0126235.

25. Jouberton, A., Shaw, T.E., Miles, E., McCarthy, M., Fugger, S., Ren, S., Dehecq, A., Yang, W., and Pellicciotti, F. (2022). Warming-induced monsoon precipitation phase change intensifies glacier mass loss in the southeastern Tibetan Plateau. Proc. Natl. Acad. Sci. USA *119*, e21097961199. https://doi.org/10.1073/pnas.2109796119.

26. Gertler, C.G., Puppala, S.P., Panday, A., Stumm, D., and Shea, J. (2016). Black carbon and the Himalayan cryosphere: A review. Atmos. Environ. *125*, 404–417. https://doi.org/10.1016/j.atmosenv.2015.08.078.

27. Li, C., Bosch, C., Kang, S., Andersson, A., Chen, P., Zhang, Q., Cong, Z., Chen, B., Qin, D., and Gustafsson, Ö. (2016). Sources of black carbon to the Himalayan-Tibetan Plateau glaciers. Nat. Commun. *7*, 12574–12577. https://doi.org/10.1038/ncomms12574.

28. Li, F., Wan, X., Wang, H., Orsolini, Y.J., Cong, Z., Gao, Y., and Kang, S. (2020). Arctic sea-ice loss intensifies aerosol transport to the Tibetan Plateau. Nat. Clim. Chang. *10*, 1037–1044. https://doi.org/10.1038/s41558-020-0881-2.

29. Sarangi, C., Qian, Y., Rittger, K., Leung, L.R., Chand, D., Bormann, K.J., and Painter, T.H. (2020). Dust dominates high-altitude snow darkening and melt over high-mountain Asia. Nat. Clim. Chang. *10*, 1045–1051. https://doi.org/10.1038/s41558-020-00909-3.

30. Feng, S., Cook, J.M., Naegeli, K., Anesio, A.M., Benning, L.G., and Tranter, M. (2024). The Impact of Bare Ice Duration and Geo-Topographical Factors on the Darkening of the Greenland Ice Sheet. Geophys. Res. Lett. *51*, e2023GL104894. https://doi.org/10.1029/2023GL104894.

31. Cook, J., Edwards, A., Takeuchi, N., and Irvine-Fynn, T. (2016). Cryoconite: The dark biological secret of the cryosphere. Prog. Phys. Geogr. *40*, 66–111. https://doi.org/10.1177/0309133315616574.

32. Vincent, C., Dumont, M., Six, D., Brun, F., Picard, G., and Arnaud, L. (2018). Why do the dark and light ogives of Forbes bands have similar surface mass balances? J. Glaciol. *64*, 236–246. https://doi.org/10.1017/jog.2018.12.

33. Azzoni, R.S., Senese, A., Zerboni, A., Maugeri, M., Smiraglia, C., and Diolaiuti, G.A. (2016). Estimating ice albedo from fine debris cover quantified by a semi-automatic method: The case study of Forni Glacier. Cryosphere *10*, 665–679. https://doi.org/10.5194/tc-10-665-2016.

34. Naegeli, K., Huss, M., and Hoelzle, M. (2019). Change detection of bare-ice albedo in the Swiss Alps. Cryosphere *13*, 397–412. https://doi.org/10.5194/tc-13-397-2019.

35. Xiao, Y., Ke, C.Q., Shen, X., Cai, Y., and Li, H. (2023). What drives the decrease of glacier surface albedo in High Mountain Asia in the past two decades? Sci. Total Environ. *863*, 160945. https://doi.org/10.1016/j.scitotenv.2022.160945.

36. Wang, J., Ye, B., Cui, Y., He, X., and Yang, G. (2014). Spatial and temporal variations of albedo on nine glaciers in western China from 2000 to 2011. Hydrol. Process. *28*, 3454–3465. https://doi.org/10.1002/hyp.9883.

37. Tang, Z., Wang, X., Deng, G., Wang, X., Jiang, Z., and Sang, G. (2020). Spatiotemporal variation of snowline altitude at the end of melting season across High Mountain Asia, using MODIS snow cover product. Adv. Space Res. *66*, 2629–2645. https://doi.org/10.1016/j.asr.2020.09.035.

38. Thakuri, S., Salerno, F., Smiraglia, C., Bolch, T., D'Agata, C., Viviano, G., and Tartari, G. (2014). Tracing glacier changes since the 1960s on the south slope of Mt. Everest (central Southern Himalaya) using optical satellite imagery. Cryosphere *8*, 1297–1315. https://doi.org/10.5194/tc-8-1297-2014.

39. Guo, Z., Geng, L., Shen, B., Wu, Y., Chen, A., and Wang, N. (2021). Spatiotemporal variability in the glacier snowline altitude across high mountain Asia and potential driving factors. Remote Sens. (Basel) *13*, 425. https://doi.org/10.3390/rs13030425.

40. Jiang, S., Nie, Y., Liu, Q., Wang, J., Liu, L., Hassan, J., Liu, X., and Xu, X. (2018). Glacier change, supraglacial debris expansion and glacial lake evolution in the Gyirong River Basin, Central Himalayas, between 1988 and 2015. Remote Sens. (Basel) *10*, 986. https://doi.org/10.3390/rs10070986.

41. Xie, F., Liu, S., Wu, K., Zhu, Y., Gao, Y., Qi, M., Duan, S., Saifullah, M., and Tahir, A.A. (2020). Upward Expansion of Supra-Glacial Debris Cover in the Hunza Valley, Karakoram, During 1990 ∼ 2019. Front. Earth Sci. (Lausanne) *8*. https://doi.org/10.3389/feart.2020.00308.

42. Brun, F., Dumont, M., Wagnon, P., Berthier, E., Azam, M.F., Shea, J.M., Sirguey, P., Rabatel, A., and Ramanathan, A. (2015). Seasonal changes in surface albedo of Himalayan glaciers from MODIS data and links with the annual mass balance. Cryosphere *9*, 341–355. https://doi.org/10.5194/tc-9-341-2015.

43. Ren, S., Miles, E.S., Jia, L., Menenti, M., Kneib, M., Buri, P., McCarthy, M.J., Shaw, T.E., Yang, W., and Pellicciotti, F. (2021). Anisotropy parameterization development and evaluation for glacier surface albedo retrieval

from satellite observations. Remote Sens. (Basel) *13*, 1714. https://doi.org/10.3390/rs13091714.

44. Zhu, M., Yao, T., Yang, W., Wu, G., Li, S., Zhao, H., and Thompson, L.G. (2022). Possible Causes of Anomalous Glacier Mass Balance in the Western Kunlun Mountains. J. Geophys. Res. Atmos. *127*, 1–20. https://doi.org/10.1029/2021JD035705.

45. Sakai, A., and Fujita, K. (2017). Contrasting glacier responses to recent climate change in high-mountain Asia. Sci. Rep. *7*, 13717–13718. https://doi.org/10.1038/s41598-017-14256-5.

46. Miles, E., McCarthy, M., Dehecq, A., Kneib, M., Fugger, S., and Pellicciotti, F. (2021). Health and sustainability of glaciers in High Mountain Asia. Nat. Commun. *12*, 2868–2877. https://doi.org/10.1038/s41467-021-23073-4.

47. Brock, B.W., Willis, I.C., and Sharp, M.J. (2000). Measurement and parameterization of albedo variations at Haut Glacier d'Arolla, Switzerland. J. Glaciol. *46*, 675–688. https://doi.org/10.3189/172756500781832675.

48. Grigholm, B., Mayewski, P.A., Aizen, V., Kreutz, K., Aizen, E., Kang, S., Maasch, K.A., and Sneed, S.B. (2017). A twentieth century major soluble ion record of dust and anthropogenic pollutants from Inilchek Glacier, Tien Shan. J. Geophys. Res. *122*, 1884–1900. https://doi.org/10.1002/2016JD025407.

49. Zheng, C., Li, Z., Zhou, P., Zhang, X., Zhou, X., and Ma, S. (2021). Physicochemical Impacts of Dust Storms on Aerosol and Glacier Meltwater on the Northern Margin of the Taklimakan Desert. Front. Earth Sci. (Lausanne) *8*, 527663. https://doi.org/10.3389/feart.2020.527663.

50. Zhu, M., Yao, T., Xie, Y., Xu, B., Yang, W., and Yang, S. (2020). Mass balance of Muji Glacier, northeastern Pamir, and its controlling climate factors. J. Hydrol. (Amst.) *590*, 125447. https://doi.org/10.1016/j.jhydrol.2020.125447.

51. Bolibar, J., Rabatel, A., Gouttevin, I., Zekollari, H., and Galiez, C. (2022). Nonlinear sensitivity of glacier mass balance to future climate change unveiled by deep learning. Nat. Commun. *13*, 409–411. https://doi.org/10.1038/s41467-022-28033-0.

52. Pellicciotti, F., Brock, B., Strasser, U., Burlando, P., Funk, M., and Corripio, J. (2005). An enhanced temperature-index glacier melt model including the shortwave radiation balance: Development and testing for Haut Glacier d'Arolla, Switzerland. J. Glaciol. *51*, 573–587. https://doi.org/10.3189/172756505781829124.

53. Azam, M.F., Kargel, J.S., Shea, J.M., Nepal, S., Haritashya, U.K., Srivastava, S., Maussion, F., Qazi, N., Chevallier, P., Dimri, A.P., et al. (2021). Glaciohydrology of the Himalaya-Karakoram. Science *373*, eabf3668. https://doi.org/10.1126/science.abf3668.

54. Naegeli, K., and Huss, M. (2017). Sensitivity of mountain glacier mass balance to changes in bare-ice albedo. Ann. Glaciol. *58*, 119–129. https://doi.org/10.1017/aog.2017.25.

55. Brock, B.W., and Arnold, N.S. (2000). A spreadsheet-based (Microsoft Excel) point surface energy balance model for glacier and snow melt studies. Earth Surf. Process. Landf. *25*, 649–658. https://doi.org/10.1002/1096-9837(200006)25:6<649::AID-ESP97>3.0.CO;2-U.

56. Liu, L., Ma, Y., Menenti, M., Su, R., Yao, N., and Ma, W. (2021). Improved parameterization of snow albedo in Noah coupled with Weather Research and Forecasting: Applicability to snow estimates for the Tibetan Plateau. Hydrol. Earth Syst. Sci. *25*, 4967–4981. https://doi.org/10.5194/hess-25-4967-2021.

57. Berthier, E., Vincent, C., Magnusson, E., Gunnlaugsson, A.T., Pitte, P., Le Meur, E., Masiokas, M., Ruiz, L., Palsson, F., Belart, J.M.C., et al. (2014). Glacier topography and elevation changes derived from Pleiades sub-meter stereo images. Cryosphere 8, 2275–2291.

58. RGI Consortium (2017). Randolph Glacier Inventory–A Dataset of Global Glacier Outlines: Version 6.0: Technical Report, Global Land Ice Measurements from Space.

59. Rounce, D.R., Hock, R., Maussion, F., Hugonnet, R., Kochtitzky, W., Huss, M., Berthier, E., Brinkerhoff, D., Compagno, L., Copland, L., et al. (2023). Global glacier change in the 21st century: Every increase in temperature matters. Science *379*, 78–83. https://doi.org/10.1126/science.abo1324.

60. Scherler, D., Wulf, H., and Gorelick, N. (2018). Global Assessment of Supraglacial Debris-Cover Extents. Geophys. Res. Lett. *45*, 11798–11805. https://doi.org/10.1029/2018GL080158.

61. Hall, D.K., Tait, A.B., Riggs, G.A., Salomonson, V.V., Chien, J.Y.L., and Klein, A.G. (1998). Algorithm Theoretical Basis Document (ATBD) for the MODIS Snow-, Lake Ice- and Sea Ice-Mapping Algorithms.

62. Ren, S., Jia, L., Menenti, M., and Zhang, J. (2023). Changes in glacier albedo and the driving factors in the Western Nyainqentanglha Mountains from 2001 to 2020. J. Glaciol. *69*, 1500–1514. https://doi.org/10.1017/jog.2023.45.

63. Wen, J., Liu, Q., Liu, Q., Xiao, Q., and Li, X. (2009). Parametrized BRDF for atmospheric and topographic correction and albedo estimation in Jiangxi rugged terrain, China. Int. J. Remote Sens. *30*, 2875–2896. https://doi.org/10.1080/01431160802558618.

64. Tadono, T., Ishida, H., Oda, F., Naito, S., Minakawa, K., and Iwamoto, H. (2014). Precise Global DEM Generation by ALOS PRISM. ISPRS Ann. Photogramm. Remote Sens. Spatial Inf. Sci. *II–4*, 71–76. https://doi.org/10.5194/isprsannals-ii-4-71-2014.

65. Liang, S. (2001). Narrowband to broadband conversions of land surface albedo I: Algorithms. Remote Sens. Environ. *76*, 213–238. https://doi.org/10.1016/S0034-4257(00)00205-4.

66. Stroeve, J., Box, J.E., Gao, F., Liang, S., Nolin, A., and Schaaf, C. (2005). Accuracy assessment of the MODIS 16-day albedo product for snow: Comparisons with Greenland in situ measurements. Remote Sens. Environ. *94*, 46–60. https://doi.org/10.1016/j.rse.2004.09.001.

67. Davaze, L., Rabatel, A., Arnaud, Y., Sirguey, P., Six, D., Letreguilly, A., and Dumont, M. (2018). Monitoring glacier albedo as a proxy to derive summer and annual surface mass balances from optical remote-sensing data. Cryosphere *12*, 271–286. https://doi.org/10.5194/tc-12-271-2018.

68. Muñoz-Sabater, J., Dutra, E., Agustí-Panareda, A., Albergel, C., Arduini, G., Balsamo, G., Boussetta, S., Choulga, M., Harrigan, S., Hersbach, H., et al. (2021). ERA5-Land: A state-of-the-art global reanalysis dataset for land applications. Earth Syst. Sci. Data *13*, 4349–4383. https://doi.org/10.5194/essd-13-4349-2021.

69. Randles, C.A., da Silva, A.M., Buchard, V., Colarco, P.R., Darmenov, A., Govindaraju, R., Smirnov, A., Holben, B., Ferrare, R., Hair, J., et al. (2017). The MERRA-2 aerosol reanalysis, 1980 onward. Part I: System description and data assimilation evaluation. J. Clim. *30*, 6823–6850. https://doi.org/10.1175/JCLI-D-16-0609.1.

70. Wang, X., Tolksdorf, V., Otto, M., and Scherer, D. (2021). WRF-based dynamical downscaling of ERA5 reanalysis data for High Mountain Asia: Towards a new version of the High Asia Refined analysis. Int. J. Climatol. *41*, 743–762. https://doi.org/10.1002/joc.6686.

71. Khanal, S., Tiwari, S., Lutz, A.F., Hurk, B.V.D., and Immerzeel, W.W. (2023). Historical Climate Trends over High Mountain Asia Derived from ERA5 Reanalysis Data. J. Appl. Meteorol. Climatol. *62*, 263–288. https://doi.org/10.1175/JAMC-D-21-0045.1.

72. Buri, P., Fatichi, S., Shaw, T.E., Miles, E.S., McCarthy, M.J., Fyffe, C.L., Fugger, S., Ren, S., Kneib, M., Jouberton, A., et al. (2023). Land Surface Modeling in the Himalayas: On the Importance of Evaporative Fluxes for the Water Balance of a High-Elevation Catchment. Water Resour. Res. *59*. https://doi.org/10.1029/2022WR033841.

73. Fugger, S., Shaw, T.E., Jouberton, A., Miles, E.S., Buri, P., McCarthy, M., Fyffe, C., Fatichi, S., Kneib, M., Molnar, P., and Pellicciotti, F. (2024). Hydrological regimes and evaporative flux partitioning at the climatic ends of High Mountain Asia. Environ. Res. Lett. *19*, 44057. https://doi.org/10.1088/1748-9326/ad25a0.

74. Shaw, T.E., Miles, E.S., Chen, D., Jouberton, A., Kneib, M., Fugger, S., Ou, T., Lai, H.W., Fujita, K., Yang, W., et al. (2022). Multi-decadal monsoon characteristics and glacier response in High Mountain Asia. Environ. Res. Lett. *17*, 104001–104013. https://doi.org/10.1088/1748-9326/ac9008.

75. Gardner, A.S., and Sharp, M.J. (2010). A review of snow and ice albedo and the development of a new physically based broadband albedo parameterization. J. Geophys. Res. *115*, 1–15. https://doi.org/10.1029/2009JF001444.

76. Ding, B., Yang, K., Yang, W., He, X., Chen, Y., Lazhu, Guo, X., Wang, L., Wu, H., and Yao, T. (2017). Development of a Water and Enthalpy Budget-based Glacier mass balance Model (WEB-GM) and its preliminary validation. Water Resour. Res. *53*, 3146–3178. https://doi.org/10.1002/2016WR018865.

77. Miles, J. (2005). R-Squared, Adjusted R-Squared. In Encyclopedia of Statistics in Behavioral Science. https://doi.org/10.1002/0470013192.bsa526.

78. Kraaijenbrink, P.D.A., Stigter, E.E., Yao, T., and Immerzeel, W.W. (2021). Climate change decisive for Asia's snow meltwater supply. Nat. Clim. Chang. *11*, 591–597. https://doi.org/10.1038/s41558-021-01074-x.

79. O'Neill, B.C., Tebaldi, C., Van Vuuren, D.P., Eyring, V., Friedlingstein, P., Hurtt, G., Knutti, R., Kriegler, E., Lamarque, J.F., Lowe, J., et al. (2016). The Scenario Model Intercomparison Project (ScenarioMIP) for CMIP6. Geosci. Model Dev. *9*, 3461–3482. https://doi.org/10.5194/gmd-9-3461-2016.

80. Eyring, V., Bony, S., Meehl, G.A., Senior, C.A., Stevens, B., Stouffer, R.J., and Taylor, K.E. (2016). Overview of the Coupled Model Intercomparison Project Phase 6 (CMIP6) experimental design and organization. Geosci. Model Dev. *9*, 1937–1958. https://doi.org/10.5194/gmd-9-1937-2016.

81. Rounce, D.R., Hock, R., and Shean, D.E. (2020). Glacier Mass Change in High Mountain Asia Through 2100 Using the Open-Source Python Glacier Evolution Model (PyGEM). Front. Earth Sci. (Lausanne) *7*. https://doi.org/10.3389/feart.2019.00331.

82. Marzeion, B., Hock, R., Anderson, B., Bliss, A., Champollion, N., Fujita, K., Huss, M., Immerzeel, W.W., Kraaijenbrink, P., Malles, J.H., et al. (2020). Partitioning the Uncertainty of Ensemble Projections of Global Glacier Mass Change. Earth's Future *8*. https://doi.org/10.1029/2019EF001470.

83. Scher, C., Steiner, N.C., and McDonald, K.C. (2021). Mapping seasonal glacier melt across the Hindu Kush Himalaya with time series synthetic aperture radar (SAR). Cryosphere *15*, 4465–4482. https://doi.org/10.5194/tc-15-4465-2021.

84. Kraaijenbrink, P.D.A., Bierkens, M.F.P., Lutz, A.F., and Immerzeel, W.W. (2017). Impact of a global temperature rise of 1.5 degrees Celsius on Asia's glaciers. Nature *549*, 257–260. https://doi.org/10.1038/nature23878.

85. Tang, Z., Deng, G., Hu, G., Zhang, H., Pan, H., and Sang, G. (2022). Satellite observed spatiotemporal variability of snow cover and snow phenology over high mountain Asia from 2002 to 2021. J. Hydrol. (Amst.) *613*, 128438. https://doi.org/10.1016/j.jhydrol.2022.128438.